Damage morphology along ion traces in Au-irradiated $Bi_2Sr_2CaCu_2O_x$

D. X. Huang* and Y. Sasaki
Japan Fine Ceramics Center, 2-4-1 Mutsuno, Atsuta-ku, Nagoya 456, Japan

S. Okayasu, T. Aruga, and K. Hojou
Japan Atomic Energy Research Institute, Tokai-mura, Ibaraki-ken 319-11, Japan

Y. Ikuhara
Department of Materials Science, University of Tokyo, Tokyo 113, Japan
(Received 13 January 1998)

We systematically observed the damage morphology along ion traces by transmission electron microscope in 230 MeV Au-irradiated $Bi_2Sr_2CaCu_2O_x$ single crystals. The results gave us a basic understanding of how high-energy ions interact with the target atoms, lose their energy, and are stopped. Three types of transitive defect morphologies, large-angle-deflected columnar defects, cascade-defect-dotted columnar defects, and ordered cascade defects, were found to be located between two typical defect morphologies, parallel columnar defects and disordered cascade defects, in different penetration depth regions. The mechanisms for the formation of these transitive defect morphologies were suggested. The analysis of ion-energy deposition in each penetration depth region and the results obtained indicated that our suggested mechanisms are reasonable. This study also supplied us with an effective experimental method to directly estimate the columnar defect size distribution versus ion penetration depth and the ion-energy thresholds to produce columnar defects and cascade defects. [S0163-1829(98)01422-2]

I. INTRODUCTION

Ion irradiation has been widely used to artificially create crystal defects in superconducting materials which can act as flux-pinning sites and prominently increase the critical current density (J_c).[1–4] Since the efficiency of irradiation-induced defects in flux pinning strongly depends on their microstructures and distributions, the morphologic study of such defects is the first important step in clarifying the origin of flux pinning in irradiated superconductors. It can also supply the basic experimental data for an understanding of the mechanism of ion-target interaction. Usually, heavy-ion beams with very high energies, e.g., several GeV, are used to produce the columnar defects for flux pinning in superconducting materials. In thin-film samples, the induced defect morphology is quite simple and can be assumed to be parallel columnar defects with a highly uniform column size within the limited thickness of the target materials. The detailed microstructure and the two-dimensional distribution on the bombarded surface for this kind of columnar defect have been intensively studied using plan-view observation methods.[5,6] For bulk samples, however, the irradiation-induced defect morphology is very complicated and we also do not have a good understanding of it now. Therefore, it is quite difficult to establish a good connection between the defect structures and their flux-pinning efficiency. Another kind of irradiation-induced defect that has been extensively studied in irradiated materials is the collision cascade defects produced by ion beams with very low energies around several MeV or less than 1 MeV. Since the ion species, the ion energies, and the target materials previously used in ion-irradiation experiments are very scattered, the conditions to generate the different kinds of irradiation-induced defects are still unclear. Until now, to our knowledge there has been no direct experimental data to describe how the defect morphology changes as the ion energy is gradually decreased in the target materials and how high-energy ions interact with the target atoms to be stopped.

In order to answer these basic questions in the ion-irradiation research field, we designed an irradiation experiment for this study. The incident ion energy we selected was 230 MeV and the incident ion was the Au ion. In this case, the ion penetration depth will be limited within 20 μm and at the same time parallel columnar defects can still be produced near the bombarded surface layer in the target materials. Therefore, if we select target materials thicker than 20 μm, the incident ions will lose their energy gradually from 230 MeV and stop in the target material. The various damage morphologies produced by ions with various energies from 230 to 0 MeV will be presented in the target material and located in different ion-penetration depth regions. By using a cross-sectional observation method, we can obtain the relationship between the irradiation-damage morphology and the incident ion energy in a large energy region.

Based on the above consideration, $Bi_2Sr_2CaCu_2O_x$ single-crystal plates ($\sim$20 μm in thickness) were irradiated using 230 MeV Au ions. Here, we report on the continuous cross-sectional observation of irradiation damage morphology from the ion bombarded surface to a depth of about 20 μm in the target crystal using transmission electron microscopy (TEM). A gradually changing process in irradiation-induced defect morphology from parallel amorphous columns to disordered collision cascades was clearly observed. Three kinds of transitive irradiation-induced defect morphologies produced by the ions in middle energy region were found and the forming mechanisms for these transitive defect mor-

phologies were suggested. Furthermore, we applied this observation method in this study to measure the columnar defect size distribution versus the ion penetration depth and to estimate the ion-energy thresholds to generate the columnar defects and cascade defects in Au-irradiated $Bi_2Sr_2CaCu_2O_x$ crystals.

II. EXPERIMENTAL

The $Bi_2Sr_2CaCu_2O_x$ single crystals used for ion irradiation were prepared using the floating-zone melting method.[7] The crystals were cleaved into thin sheets of about 20 μm thickness along the *a*-*b* plane and cut to about 1-mm wide and 2-mm long. Perpendicular to the surface of the thin sheets, 230-MeV Au-ion irradiation was performed with a dose of 9.7×10^{10} ions/cm^2 at room temperature using a Tandem accelerator at the Japan Atomic Energy Research Institute. Cross-sectional samples for TEM observation were prepared by pasting the ion-irradiated samples between silicon pellets and cutting them into slices along the *a* or *b* axis of the crystal. The slices were then mechanically ground to 40–50 μm, dimpled to about 10 μm, and finally ion-milled with a liquid-nitrogen cold stage. The TEM analyses of damage morphology along the ion traces were performed using a Topcon EM-002B high-resolution TEM operated at 200 keV.

A high-energy-extended EDEP-1 computer code[8] was used to calculate the damage depth profile of high-energy heavy ions in the target material. Using this software, the distributions for stopping power and ion residual energy against the penetration depth were estimated. The energy transference in the nuclear collision between high-energy incident ions and target atoms was calculated based on the rigid-ball elastic collision model. In the formation of cascade defects, a method[9] based on Boltzmann transport theory and the thermal spike model was employed to estimate the energy transference from the incident ions to primary knock-on atoms (PKA's).

III. RESULTS AND DISCUSSIONS

A. Defect morphologies along ion traces

Figure 1 is a series of bright-field images taken along the ion penetration path in the 230 MeV Au-irradiated $Bi_2Sr_2CaCu_2O_x$ crystal. It shows the change in the irradiation-induced defect morphology as the Au ions penetrate through the target material. Between the two typical ion-irradiation-induced defect morphologies (parallel columnar defects and disordered cascade defects), we found three types of transitive defect morphologies which we named large-angle-deflected columnar defects, cascade-defect-dotted columnar defects, and ordered cascade defects. The detailed distribution state for all the defect morphologies can be described as follows. (1) *Parallel columnar defects*. Near the irradiated surface layer, the defects generated by such high-energy incident ions are amorphous columns with almost parallel orientation along the ion incident direction. As they penetrate into the target, the ions slow down through interaction with the target electrons and/or atoms. The size of the produced amorphous column also gradually decreases. (2) *Large-angle-deflected columnar defects*. Starting from a depth of 2 μm, we found a few columnar defects to be deflected from the ion incident direction with angles larger than 30°. As the ions penetrated deeper, the density for this kind of large-angle-deflected columnar defect was found to increase. (3) *Cascade-defect-dotted columnar defects*. When the ions penetrated to a depth of about 5 μm and their energy was reduced to some specific value, we found a region in which the columnar and cascade defects coexisted and the cascade defects were distributed in order along the axes of the columnar defects. (4) *Ordered cascade defects*. As ion energy decreased further in the target crystal, the continuous columnar defects disappeared and, instead, a kind of cascade defect with a tail appeared. We found that this kind of cascade defect with a tail arranged in lines along the extended direction of the tails. (5) *Disordered cascade defects*. After the appearance of ordered cascade defects, only pure disordered spherical cascade defects were found to exist in the target material. When the ions penetrated deeper, the density of the cascade defects gradually decreased. Finally, when the ions penetrated deeper than 11 μm, no cascade defects could be observed by TEM.

B. Energy thresholds to produce five kinds of defect morphologies

It is well known that the morphology of irradiation-induced defects strongly depends on the mechanism of ion-target interaction. Up to now, only two types of defects have been observed by TEM in ion-irradiated materials. The first is amorphous columnar defects in the ion incident direction. The corresponding mechanism for ion energy deposition in target materials is called electronic energy deposition (S_e), which results from the ionizations and/or electronic excitations of target atoms induced by high-energy ions. The second is cascade defects which are generated by low-energy ions through nuclear collisions with target atoms. This process of ion-energy deposition is called nuclear energy deposition (S_n). According to the existing experimental knowledge, the parallel columnar defects are produced by heavy ions with energies from several hundred MeV to several GeV and the cascade defects are produced by incident ions with energies around 1 MeV. These two types of defects produced by energetic ions with very different energies have only been observed separately. Even though the thresholds of ion energy and stopping power for producing both kinds of defects have often been mentioned,[10,11] detailed experimental data for an understanding of such thresholds have not been obtained until now. The continuous observation of defect distribution along the ion traces in this study has provided us with direct experimental data allowing us to understand these energy thresholds and the relationship between them in the Au-irradiated $Bi_2Sr_2CaCu_2O_x$ single crystal.

From the TEM observation results in Fig. 1, we can clearly see that the columnar defects exist in a depth region ranged from the ion-bombarded surface to a depth of about 7.5 μm. The depth region where the cascade defects are located is found to be from 5 to 11 μm. Using a high-energy extended EDEP-1 code,[8] the lower limits of stopping power (dE/dx) and ion residual energy were estimated to be about 16 MeV/μm and 50 MeV/ion, respectively, to produce the visible columnar defects in Au-irradiated $Bi_2Sr_2CaCu_2O_x$

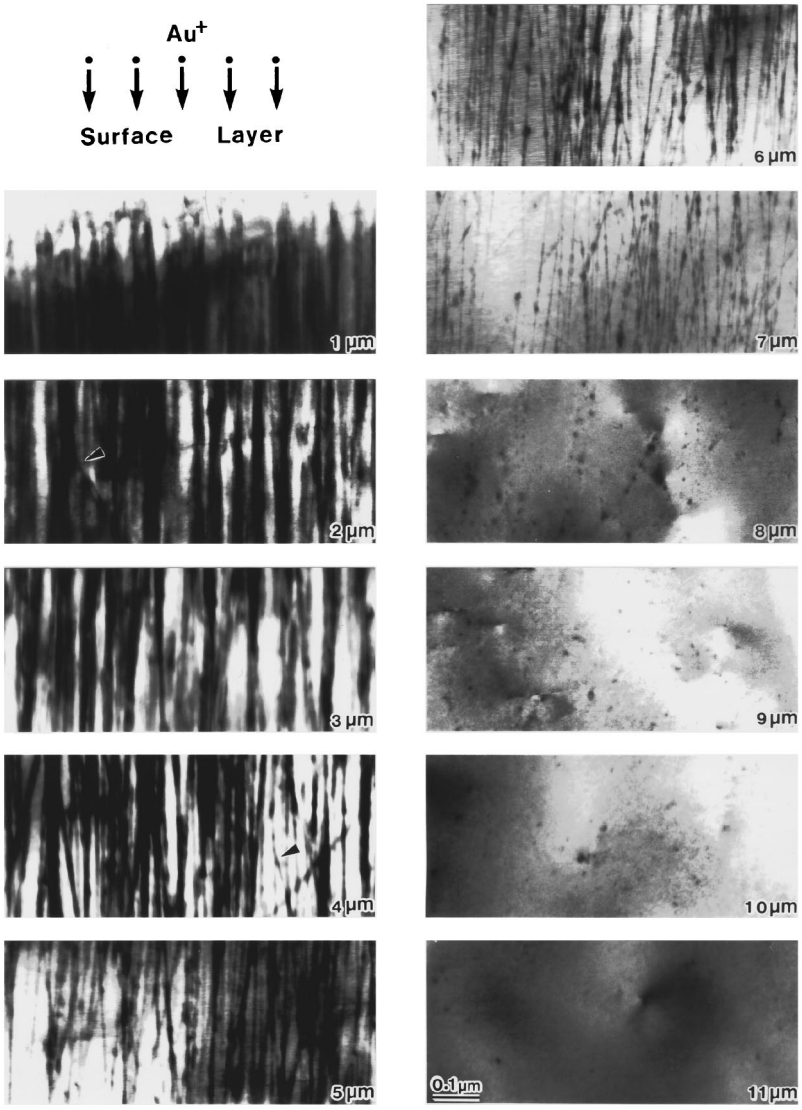

FIG. 1. A series of bright-field images picked out at an equal distance from the continuously observed images along the ion trace. The corresponding depth from the ion bombarded surface for each image is presented at the bottom corner. The black triangles show the large-angle-deflected columnar defects.

single crystal. This value agrees well with the lower thresholds of electronic energy-loss rate reported by Leghissa *et al.*[12] and by Kumakura *et al.*[13] Furthermore, the estimated regions for dE/dx and ion residual energy to produce the visible cascade defects in the $Bi_2Sr_2CaCu_2O_x$ crystal ranged approximately from 22 to 8 MeV/μm and from 100 to 10 MeV/ion.

Two different morphologies for pure columnar defects produced by high-energy heavy ions were observed in this study. The first is the pure parallel columnar defects that were previously reported, which are located within a depth region from the ion-bombarded surface to a depth of about 2 μm. In the depth region from 2 to 7.5 μm, another kind of columnar defect was found to be deflected at a large angle from the ion incident direction, and two kinds of columnar defects were mixed in this depth region. The estimated lower ion energy threshold to produce pure parallel columnar defects was 170 MeV/ion and the corresponding lower limit of stopping power was about 27 MeV/μm. The regions for ion energy and stopping power to produce the mixed morphology for the two types of columnar defects ranged from 170 to 50 MeV/ion and from 27 to 16 MeV/μm, respectively.

In the changing process of defect morphology, there was a depth region where two kinds of columnar defects coexisted with cascade defects, which could clearly be observed in the Au-irradiated $Bi_2Sr_2CaCu_2O_x$ crystal in this study. The special energy region to produce such defect morphology ranged from 100 to 50 MeV/ion and the corresponding region for stopping power ranged from 22 to 16 MeV/μm. In this energy region, we could observe three kinds of defect morphologies, parallel columnar defects, large-angle-deflected columnar defects, and cascade defects. This implies that three different kinds of ion-target interaction mechanisms can work in the same energy region. The cascade collisions can not only take place in the low-energy region, but they can also take place in the high-energy region (e.g., 100 MeV/ion) where the columnar defects can still be produced.

In the pure cascade defect area, the defect morphology is also not only of one kind. Except for the typical disordered cascade defect morphology, there was another ordered cas-

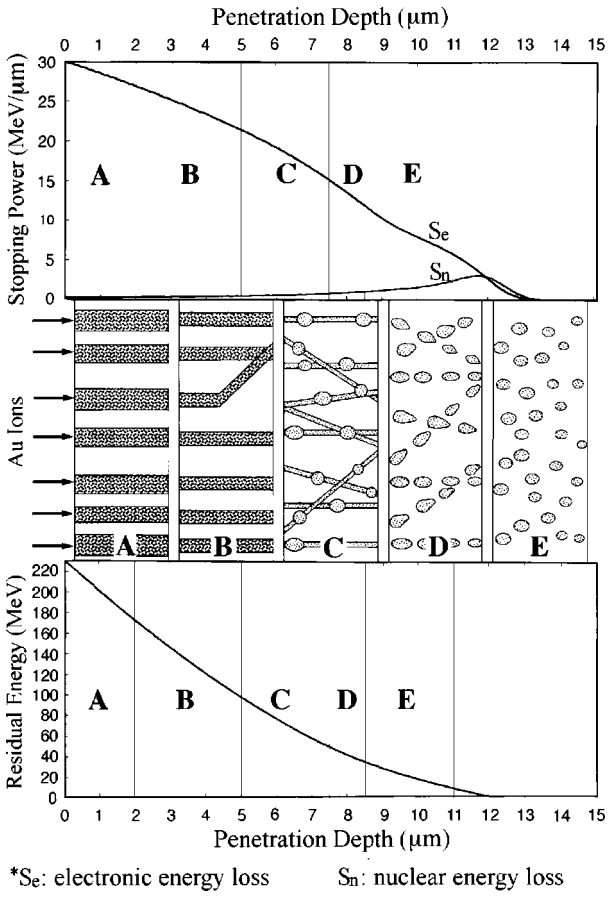

FIG. 2. A schematic showing five kinds of irradiation-induced defect morphologies in different ion-energy regions. The attached curves are the depth profile calculation results using high-energy extended EDEP-1 code which showed the changing process of stopping power (up side) and ion residual energy (down side) as the penetration depth increases gradually in the target material.

cade defect morphology in the target crystal when the ion energy was just a bit higher than the ion energy to produce disordered cascade defects. The regions of ion residual energy and dE/dx to produce ordered cascade defects ranged, respectively, from 50 to 36 MeV/ion and from 16 to 13 MeV/μm. To produce pure disordered cascade defects, the ion energy and dE/dx should be lower than 36 MeV/ion and 13 MeV/μm.

Figure 2 is a schematic for showing the five kinds of defect morphologies distributed along the ion traces in detail. In order to get a clearer impression of the energy conditions to produce these defects, the depth profiles for stopping power and ion residual energy estimated by EDEP-1 code are attached above and below the schematic. Table I shows the detailed data of the distribution regions for penetration depth, ion residual energy, and stopping power to produce each kind of defect morphology.

C. Depth distribution of columnar defect size

Although clarifying the distribution of columnar defect size versus dE/dx is very arduous, it has to be done because it is a necessary step in clarifying the process of electronic energy deposition of incident ions in the target material. For only a few target materials such as mica, $Y_3Fe_5O_{12}$ and $YBa_2Cu_3O_{7-\delta}$, the distribution curves of columnar defect size versus dE/dx have been given by summarizing all the extant related experimental data.[11,14,15] However, there is insufficient experimental data to plot such a curve for $Bi_2Sr_2CaCu_2O_x$ crystal. The continuous observation of columnar defects along the ion traces done in this study seems a very effective means to acquire the data to plot such a distribution curve. Since ion energy and dE/dx continuously change along the ion traces, theoretically, we can obtain a continuous distribution for columnar defect size versus dE/dx or ion energy using one irradiated sample. Also we do not need to consider experimental errors from different incident ions, different target materials, and so on. In this study the columnar defect size at each penetration depth was measured using high-resolution electron microscope (HREM) images taken in the same depth region. The distribution curve obtained for columnar defect size versus penetration depth is shown in Fig. 3(a). Using high-energy extended EDEP-1 software,[8] we can calculate the dE/dx and ion energy at each penetration depth in the target material. Therefore, we can also easily obtain the correlation of columnar size with dE/dx or ion residual energy. Figure 3(b)

TABLE I. Regions of ion penetration depth, ion energy, and stopping power for generating five kinds of defect morphologies.

Depth (μm)	0 → 2	→ 5	→ 7.5 → 8.5	→ 11
Au-ion Energy (MeV)	230 → 170	→ 100	→ 50 → 36	→ 10
Stopping Power (MeV/μm)	30 → 27	→ 22	→ 16 → 13	→ 8
Parallel Columnar Defects	●	●	●	
Large-angle-deflected Columnar Defects		●	●	
Ordered Cascade Defects			●	●
Disordered Cascade Defects				●
Morphologies of Irradiation Damage	Pure Paral. Col. Def.	Mixed Col. Def. (Paral.+ Deflected)	Cas.-dotted Col. Def.	Ordered Cas. Def. / Disordered Cas. Def.

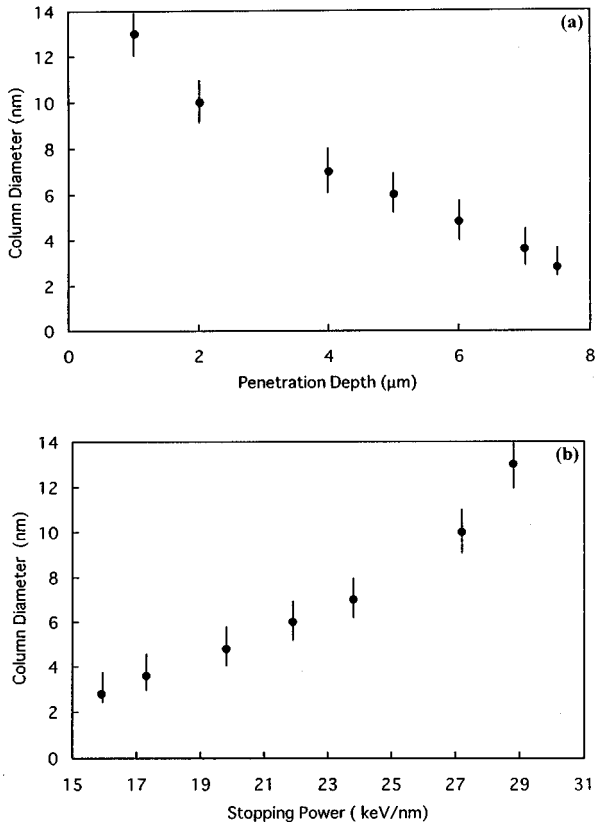

FIG. 3. Distributions of columnar defect size versus (a) ion penetration depth and (b) stopping power measured by HREM images. The value of stopping power in each penetration depth is given by the curve (up side) presented in Fig. 2.

shows the columnar size distribution against dE/dx. If we do a linear extrapolation of this curve to a high dE/dx value of 31.5 MeV/μm, the corresponding columnar size will be about 16.3 nm. This value coincides quite well with the columnar defect size (16 nm) observed by Zhu *et al.*[5] in 300 MeV Au-ion-irradiated $Bi_2Sr_2CaCu_2O_x$ crystals.

D. Discussion of mechanism for transitive defect morphologies

1. Large-angle-deflected columnar defects

It has been well known that pure parallel columnar defects are produced by an interaction process between incident ions and target electrons. Through this process, a great deal of ion energy is instantly transferred to the target electrons and the energy of the excited electrons is very quickly converted into the thermal energy of the lattice in a very localized region. When the local temperature of the lattice is higher than its melting point, a localized melting region will be formed. As a result, an amorphized zone can be observed by TEM. For a high-energy moving ion, a continuous amorphous columnar defect along the ion penetration path will be produced in the target crystal. However, there has been a very limited understanding for the nuclear collision of a high-energy incident ion with target atoms and the corresponding damage produced in the target material. We only know that the possibility of nuclear collision between high-energy ions and target atoms is not zero, theoretically.

The large-angle-deflected columnar defects observed in this study provided us with important information allowing us to understand the nuclear collision of incident ions with target atoms in the high-energy region. As shown in Table I, this energy region ranged approximately from 170 to 50 MeV. It is very easy to understand that the density of the deflected columnar defects increased with the increase in the ion penetration depth (Fig. 1). This is because as the ions penetrate into the target material, the ion energy and velocity gradually decrease, thus the mean free path for this kind of nuclear collision decreases and the collision probability is higher. Finally, it will result in a higher density for the deflected columns in the target materials.

As Fig. 1 shows, there is not an obvious melting area (amorphous area) around the collision site which can be observed by TEM. This implies that the energy transferred to the crystal lattice is very little at the moment of collision. Therefore, we can approximately consider this kind of collision to be an elastic collision. Using the rigid-ball collision model, we briefly estimated the ion deflection angle, the energy transference, and the probable defect morphology produced by this kind of collision. The result indicates that the deflected columnar defects with a deflection angle of larger than 30° are produced by the collisions between Au ions and heavy target atoms, Bi atoms. For a collision to produce a 32° deflected columnar defect as shown in the TEM image taken at a penetration depth of about 2 μm (Fig. 1), the residual energy of the deflected Au ion and the transferred energy from the Au ion to the Bi atom in this collision was estimated to be about 125 and 45 MeV, respectively. The average Au ion energy in this depth region is about 170 MeV. According to the analyses of the ion energy and the corresponding stopping power in the target material, the secondary Bi ion with an energy of 45 MeV is insufficient to produce a visible columnar defect in the $Bi_2Sr_2CaCu_2O_x$ crystal. The defect morphology around the collision area should be as that schematized in Fig. 5(b). The TEM observation results in Fig. 1 also confirmed this fact. There was only a deflected columnar defect and no accompanying columnar defect produced by an ionized Bi atom in the collision area. Concerning the lighter target atoms such as Sr, Cu, Ca, and O, the collisions of Au ions with them only caused a small-angle scattering ($<10°$) of the incident Au ions. Detailed analyses on the nuclear collision between high-energy ions and target atoms will be reported elsewhere.

The density of this kind of high-energy nuclear collision has been also briefly estimated for the Au incident ions in the depth region around 2 μm. In this estimation, the ion energy we used was 170 MeV and the nuclear stopping power estimated by the EDEP-1 software was about 0.314 MeV/μm. If we suppose that all the nuclear collisions in this ion energy region are strong collisions and the ion energy loss for each collision is about 45 MeV as analyzed above, the collision density will be about 6.77 collisions/μm^3 in an irradiation experiment with an ion dose of 9.7×10^{10} ions/cm^2. In other words, the density of target atoms displaced by this kind of nuclear collision is 6.77 atoms/μm^3 and the corresponding displaced atom ratio is about 1.0×10^{-7}. For TEM observation, this collision density is quite low and the corresponding crystal defects (large-angle-deflected columnar defects) induced by this kind of collision are also quite difficult to observe in a high ion-energy region such as that around 170 MeV, which has been confirmed in this study.

FIG. 4. HREM image showing the structural detail of the cascade-defect-dotted columnar defect. The black triangles indicate the positions of cascade defects and the arrow shows the ion penetration direction. The columnar defect can be seen clearly between two cascade defects.

2. Cascade-defect-dotted columnar defects

It was found that columnar and cascade defects coexisted in a depth region from about 5 to 7.5 μm and the cascade defects were only distributed along the axes of the columnar defects (Fig. 1). In this depth region, the corresponding ion energy ranges from 100 to 50 MeV. This kind of on-axis cascade defect had a similar shape and microstructure to the pure cascade defects produced by low-energy ions.[16–18] Therefore, the generation mechanism should also be the same and one dotted cascade defect should result from one PKA. As to their special distribution state, there is only one way to understand it: the cascade defects that appear at one columnar axis must be produced by the same ion that generates the columnar defect itself. This implies that the complete cascade-defect-dotted columnar defect is originally one single defect which is inseparable. This kind of defect morphology corresponds to the alternative energy-deposition process of electronic excitation and nuclear collision.

Figure 4 shows the detailed microstructure for this kind of irradiation-induced defect morphology. The sizes of the cascade defects distributed on the column axis are about 8 nm in diameter. In order to further explain the formation mechanism for the cascade-defect-dotted columnar defects, the deposited ion energy and the possible deflection-angle of the incident ion in the on-axis cascade collision has been analyzed in this study. Considering the healing effect in the formation of cascade defects, the volume of the damaged area we used in the analysis is about three times as that observed by TEM. By using a method[9] based on Boltzmann transport theory and the thermal spike model, the deposited energy of the incident ion to produce an 8 nm spherical cascade defect is estimated to be about 16.8 keV. This value of deposited energy is quite small compared with the original ion energy (100–50 MeV). For one cascade collision, the energy transferred from the incident ion to the PKA is less than 0.1% of the original ion energy.

Furthermore, we estimated the ion deflection angle produced by this kind of high-ion-energy cascade collision. In the estimation, when we take the heaviest target atoms (Bi) as PKA's, the possible ion-deflection angle is less than 1.5°. If the lighter atoms, such as Sr, Ca, Cu, and O, are considered to be the PKA's, the deflected angle for the incident ion will be smaller and less than 1°. The average deflection angle of incident Au ions induced by all probably occurring cascade collisions has been calculated to be about 0.6°. Since the deflection angle induced by cascade collisions in this high ion-energy region is too small, and also the direction of ion deflection by each on-axis cascade collision is random, for TEM observation the defect morphology should look like one straight columnar defect with many cascade defects distributed along the column axis. These results indicate that our original suggestion for the mechanism to produce cascade-defect-dotted columnar defects is reasonable.

It should be noted that this kind of mechanism in ion-target interaction only works in a specific region of ion energy which ranges from the upper threshold for producing cascade defects to the lower threshold for generating columnar defects, according to the distribution region for such new defects confirmed by TEM observation. For $Bi_2Sr_2CaCu_2O_x$ single crystal irradiated by Au ions, this energy region ranges approximately from 100 to 50 MeV/ion. Figure 5(c) is a schematic which can help us to further understand this mechanism.

3. Ordered and disordered cascade defects

Around a depth of 8 μm, ordered cascade defects with long tails can be found after the appearance of cascade-defect-dotted columnar defects (Fig. 1). All the cascade defects are arranged along many straight lines and the tail of each cascade defect is oriented along these lines. This kind of ordered cascade defect line can be understood as a continuity of cascade-defect-dotted columnar defects. As the ion energy decreases further, the sizes of columnar defects become smaller and smaller. The continuous columnar defects cannot be directly observed. However, when the columnar damaged area overlaps the spherical damaged area produced by a cascade collision, a trace of the columnar defect still appears in the form of a tail for each cascade defect. The mechanism to produce such ordered cascade defects should be similar to the mechanism to produce cascade-defect-dotted columnar defects, and one ordered cascade defect line should also be produced by one incident ion. The same analyses as on cascade-defect-dotted columnar defects were also carried out. The results indicated that the deflection angle of the incident ion produced by each cascade collision in this ion energy region (about 50–36 MeV) was less than 2°. If we consider the random distributions for the directions

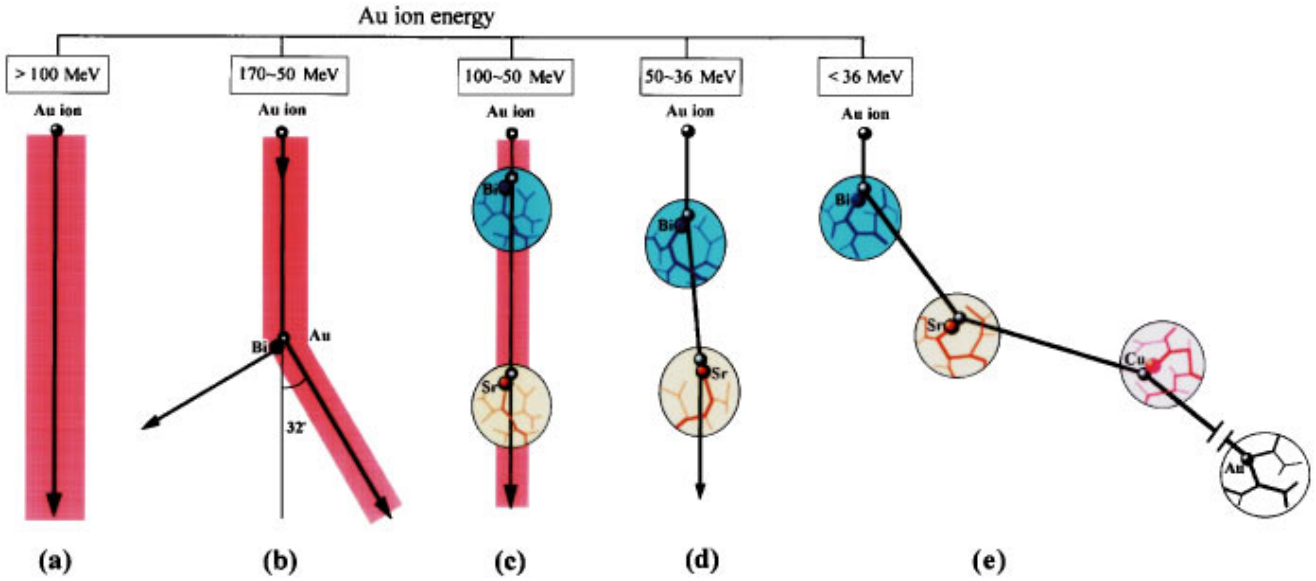

FIG. 5. (Color) Suggested models to briefly describe the mechanisms in forming the five kinds of defect morphologies produced by Au ions in different energy regions. (a) is for parallel columnar defects, (b) for large-angle-deflected columnar defects, (c) for cascade-defect-dotted columnar defects, (d) for ordered cascade defects, and (e) for disordered cascade defects.

of ion deflections in cascade collisions, it is reasonable to expect that a morphology of ordered cascade defects can be observed by TEM. The mechanism producing ordered cascade defects is schematized in Fig. 5(d).

As the ion energy decreased further, the deflection angles of incident ions induced by cascade collisions became larger and larger. The ordered cascade defect lines could barely be observed again, instead, only a disordered cascade-defect morphology could be observed. After several cascade collisions, the ion residual energy will decrease to a value, for example, of less than 100 keV. The incident ion will behave like one simple PKA producing a cascade defect by itself and finally it will stop in the target crystal. Therefore, as more and more incident ions stop in the target crystal, the density of the disordered cascade defects also decreases. Finally, no defects could be observed by TEM as Fig. 1 shows.

IV. CONCLUSIONS

Continuous TEM cross-sectional observation along the ion traces in the Au-irradiated $Bi_2Sr_2CaCu_2O_x$ crystals in this study clearly showed the process of change in irradiation-damage morphologies as the ion energy decreased, and it also supplied the direct experimental data to understand the mechanism of ion-target interaction in each energy region of incident ions. It revealed that the columnar defect morphology was not only parallel amorphous columnar defects as previously reported, but it also appeared in other morphologies, such as large-angle-deflected columnar defects and cascade-defect-dotted columnar defects. This kind of large-angle-deflected columnar defect resulted from the near-elastic collision of high-energy ions with the target atoms. And the cascade-defect-dotted columnar defects were generated by the alternative energy deposition of electronic excitation and nuclear collision. There was also more than one kind of morphology for the cascade defects. As the ion energy changes in the target material, the defect morphology also changes. In the high-energy region, the cascade defects have an ordered distribution along the direction of ion movement. Even though the ion energy is high enough to create a columnar defect, cascade defects can also be produced. These cascade defects produced by such high-energy ions were found to be distributed in order along the axis of the columnar defect. As the ions lose their energy in the target material, the size of the produced columnar defects decreases. When the size of a produced columnar defect is so small that it can hardly be observed by TEM and at the same time the ion energy is still quite high compared with the transferred energy in each cascade collision, the ion-damage morphology appears in the form of ordered cascade-defect lines. Further, all the cascade defects located on one column axis or on one straight line should be produced by one incident ion, which was suggested in this study. Subsequently, when the ion energy becomes increasingly lower, the ion-deflected angle induced by each cascade collision becomes increasingly larger and the distribution of cascade defects gradually become disordered. The calculation of ion energy deposition and the deflection angles of incident ions in the cascade collisions done in the study strongly supported our suggested mechanisms for ion-target interaction in each ion-energy region.

ACKNOWLEDGMENTS

This work was partially supported by the New Energy and Industrial Technology Development Organization (NEDO) through the International Superconductivity Technology Center (ISTEC).

*Author to whom correspondence should be sent. Electronic address: dxhuang@iname.com

[1] B. Roas, B. Hensel, G. Saemann-Ischenko, and L. Schultz, Appl. Phys. Lett. **54**, 1051 (1989).

[2] J. R. Thompson, Y. R. Sun, H. R. Kerchner, D. K. Christen, B. C. Sales, B. C. Chakoumakos, A. D. Marwick, L. Civale, and J. O. Thompson, Appl. Phys. Lett. **60**, 2306 (1992).

[3] R. C. Budhani, Y. Zhu, and M. Suenaga, Appl. Phys. Lett. **61**, 985 (1992).

[4] J. A. Cutro, D. A. Rudman, T. P. Orlando, R. B. Van Dover, L. F. Schneemeyer, A. E. White, E. M. Gyorgy, J. V. Waszczak, and R. J. Felder, Appl. Phys. Lett. **62**, 759 (1993).

[5] Y. Zhu, Z. X. Cai, R. C. Budhani, M. Suenaga, and D. O. Welch, Phys. Rev. B **48**, 6436 (1993).

[6] H. Dai, S. Yoon, J. Liu, R. C. Budhani, and C. M. Lieber, Science **256**, 1552 (1994).

[7] Y. Kubo, K. Michishita, Y. Higashida, M. Mizuno, H. Yokoyama, N. Shimizu, E. Inukai, N. Kurada, and H. Yoshita, Jpn. J. Appl. Phys., Part 2 **28**, L606 (1989).

[8] T. Aruga, K. Nakata, and S. Takamura, Nucl. Instrum. Methods Phys. Res. B **33**, 748 (1988).

[9] R. S. Averback, J. Nucl. Mater. **216**, 49 (1994).

[10] B. Hensel, B. Roas, S. Henke, R. Hopfengärtner, M. Lippert, J. P. Ströbel, M. Vildic, G. Saemann-Ischenko, and S. Klaumünzer, Phys. Rev. B **42**, 4135 (1990).

[11] M. Toulemonde, S. Bouffard, and F. Studer, Nucl. Instrum. Methods Phys. Res. B **91**, 108 (1994).

[12] M. Leghissa, T. Schuster, W. Gerhäuser, S. Klaumünzer, M. R. Koblischka, H. Kronmüller, H. Kuhn, H.-W. Neumüller, and G. Saemann-Ischenko, Europhys. Lett. **19**, 323 (1992).

[13] H. Kumakura, H. Kitaguchi, K. Togano, H. Maeda, J. Shimoyama, S. Okayasu, and Y. Kazumata, J. Appl. Phys. **74**, 451 (1993).

[14] T. A. Tombrello, Nucl. Instrum. Methods Phys. Res. B **95**, 232 (1995).

[15] J. Provost, C. Simon, M. Hervieu, D. Groult, V. Hardy, F. Studer, and M. Toulemonde, MRS Bull. **20**, 22 (1995).

[16] W. L. Zhou, Y. Sasaki, and Y. Ikuhara, Physica C **234**, 323 (1994).

[17] N. Sekimura and S. Ishino, Radiat. Eff. Defects Solids **124**, 109 (1992).

[18] S. Ishino and N. Sekimura, Ann. Chim. (Paris) **16**, 341 (1991).